INTERNATIONAL JOURNAL OF AUTOMOTIVE AND MECHANICAL ENGINEERING
ISSN: 2229-8649 e-ISSN: 2180-1606
VOLUME 22, ISSUE 2, 2025, 12373 - 12387
DOI: https://doi.org/10.15282/ijame.22.2.2025.10.0947

RESEARCH ARTICLE

Computational Fluid Dynamics Analysis of Aerodynamic Characteristics on Overtaking Vehicles in Crosswind Conditions

M. Syafiq[1], I. A. Ishak[1,*], M. Arafat[1], R. A. Rashid[2], N. E. Othman[3], Z. M. Salleh[4], S. F. Z. Abidin[1]

[1]Faculty of Engineering Technology, University of Tun Hussein Onn Malaysia, Education Hub, Pagoh, 84600, Johor
[2]Department of Chemical Engineering, The University of Manchester, Manchester, M13 9PL, UK
[3]School of Mechanical Engineering, College of Engineering, Universiti Teknologi MARA, 40450 Shah Alam, Selangor
[4]Faculty of Mechanical Engineering, Universiti Tun Hussein Onn Malaysia, Persiaran Tun Dr. Ismail, 86400 Parit Raja, Johor

ABSTRACT – Drivers frequently adjust their path due to crosswinds and overtaking, where adjacent vehicles significantly alter airflow. This study uses computational fluid dynamics to analyze the aerodynamic impact of overtaking maneuvers on simplified car models (Ahmed Bodies) under crosswind conditions. The investigation focuses on how drag, lift, and side force coefficients change during different overtaking stages at varying crosswind angles (0°, 15°, 30°, and 45°). The study focused on 2 Ahmed Body models, which are overtaking vehicle(A) and overtaking vehicle(B), in 5 different cases: before overtake, initiation of overtake, mid-overtake, completion of overtake, and after overtake. Results show that at a 15° crosswind, Car A has a higher drag coefficient (C_d: 0.3916), reducing performance and stability. At 30°, Car A shows a high lift coefficient (C_l: 0.9881); at 45°, Car B experiences a significant increase in side force coefficient (C_s: 3.1192). This is due to the pressure contour at the front corner of the vehicle surface and the vortex formation on the leeward side of the vehicles as yaw angles rise. Results show that crosswinds significantly increase aerodynamic forces and alter flow structures around vehicles. Specifically, the relative position of vehicles during overtaking greatly influences these forces, affecting vehicle stability.

ARTICLE HISTORY
Received : 28th July 2024
Revised : 17th Apr. 2025
Accepted : 02nd May 2025
Published : 12th June 2025

KEYWORDS
Overtaking maneuver
Crosswind
Aerodynamic loads
Flow structure
Vortex generation
CFD

1. INTRODUCTION

Crosswinds and overtaking maneuvers represent critical driving scenarios where aerodynamic forces can significantly compromise vehicle safety, contributing to a notable percentage of highway accidents [1], [2], [3]. Crosswinds introduce strong lateral aerodynamic loads that can destabilize vehicles, causing abrupt lane deviations, increased steering effort, or even accidents. These effects are especially critical for lightweight vehicles, trucks, and high-profile vehicles, where lateral forces can significantly impair handling [4]. During overtaking maneuvers, aerodynamic interactions between the overtaking and overtaken vehicles disturb the surrounding airflow, leading to complex pressure distributions, vortex formations, and unsteady aerodynamic forces [5]. The presence of crosswind conditions during overtaking further complicates these flow phenomena, potentially amplifying risks to vehicle stability [2], [6], [7], [8], [9], [10]. Thus, understanding the combined aerodynamic behavior during overtaking under crosswind conditions is essential for ensuring vehicle safety. Several studies have independently explored aerodynamic phenomena under either crosswind or overtaking conditions. Early investigations by Noger et al. [11] highlighted that passing maneuvers introduce transient aerodynamic loads that can affect vehicle trajectory, which is also supported by the result found in reference [12]. More recent studies, such as those by Yudianto et al., have examined crosswind impacts but focused only on isolated vehicles without considering the dynamic effects of overtaking [5]. Su et al. evaluated aerodynamic responses at different yaw angles but did not model overtaking interactions [13]. Meanwhile, Nakashima et al. conducted overtaking simulations under steady headwind conditions, neglecting the critical influence of yaw angles caused by crosswinds [14].

Further analysis by Marshall et al. explored overtaking simulations under close-proximity conditions, yet their modeling did not incorporate the effects of yaw angles induced by crosswinds, which are pertinent to understanding how vehicles behave when subjected to dynamic flow modifications [15]. This aspect is vital since crosswinds can generate complex aerodynamic responses, including nonlinear forces that can destabilize vehicles effectively [16]. Correspondingly, Liu et al. conducted simulations that discerned the crosswind's significant effects on aerodynamic forces during the overtaking process, showing the adverse implications on stability and safety experienced by the overtaken vehicle [17]. Simplified vehicle models, particularly the Ahmed Body, have been widely used in previous research to understand fundamental aerodynamic behaviors such as wake formation, flow separation, and vortex shedding. Previous studies have provided valuable insights into the aerodynamic characteristics of bluff bodies [18], [19]. The implications of crosswind conditions on the Ahmed Body's aerodynamic performance have been explored in studies like that of Sun et al., which examined how varying wind patterns affect the vehicle's aerodynamics during transient conditions [20]. Their studies primarily investigated steady-state conditions, presenting a controlled environment that aids in isolating the effects

***CORRESPONDING AUTHOR | I. A. Ishak** | ✉ izuan@uthm.edu.my

of design features on aerodynamic performance. However, this environment does not fully reflect real driving conditions, particularly those involving transient dynamics such as overtaking maneuvers in crosswind scenarios.

Despite these valuable contributions, significant gaps remain in the current literature. Much of the existing research has relied on stationary vehicle assumptions, neglected yaw angle variations during overtaking maneuvers, and overlooked the detailed interaction between wake structures of two closely passing vehicles under crosswinds [21], [22]. These limitations restrict the understanding of aerodynamic instabilities experienced during real-world overtaking, especially when vehicles encounter varying crosswind intensities. To address these gaps, the present study aims to comprehensively analyze the aerodynamic characteristics of vehicles during overtaking maneuvers under different crosswind yaw angles using computational fluid dynamics (CFD) simulations. The Ahmed Body model is utilized due to its ability to replicate key bluff-body aerodynamic phenomena while maintaining computational simplicity. The study systematically examines the effects of yaw angles of 0°, 15°, 30°, and 45°, representing realistic crosswind scenarios typically encountered on highways. The specific objectives are to quantify the variations in drag, lift, and side force coefficients during overtaking, to analyze the changes in pressure distribution, vortex formation, and flow separations, and to evaluate the aerodynamic instabilities induced by crosswind and overtaking interactions with the aim of providing practical recommendations for enhancing vehicle stability.

The structure of this paper is as follows: Section 2 describes the materials and methods, including the simulation setup, computational domain, boundary conditions, and meshing strategies. Section 3 presents and discusses the results related to aerodynamic loads, flow field properties, and structural behavior under different crosswind conditions. Finally, Section 4 concludes the findings and suggests avenues for future aerodynamic performance improvements in vehicle design.

2. METHODOLOGY

Figure 1 outlines the overall roadmap of the CFD analysis used in this study. The process begins with the development of the vehicle geometry using the Ahmed Body model, a widely accepted benchmark in external aerodynamics research due to its ability to replicate essential bluff-body flow characteristics such as wake formation, separation, and vortex shedding. Following geometry creation, the computational domain is defined within ANSYS Fluent, where boundary conditions and enclosure dimensions are carefully specified to minimize numerical blockage and ensure realistic flow development. Meshing is performed using a hybrid unstructured grid with local refinement near the vehicle surfaces and wake regions. Boundary layer meshing is applied via prism layers to accurately capture near-wall gradients. A mesh independence study is conducted using three levels of mesh density coarse, medium, and fine, to ensure that aerodynamic coefficients, particularly drag, converge with increasing mesh resolution. Figure 2 presents the results of the mesh sensitivity analysis, demonstrating that the fine mesh produces drag coefficient values in close agreement with validated results from prior studies.

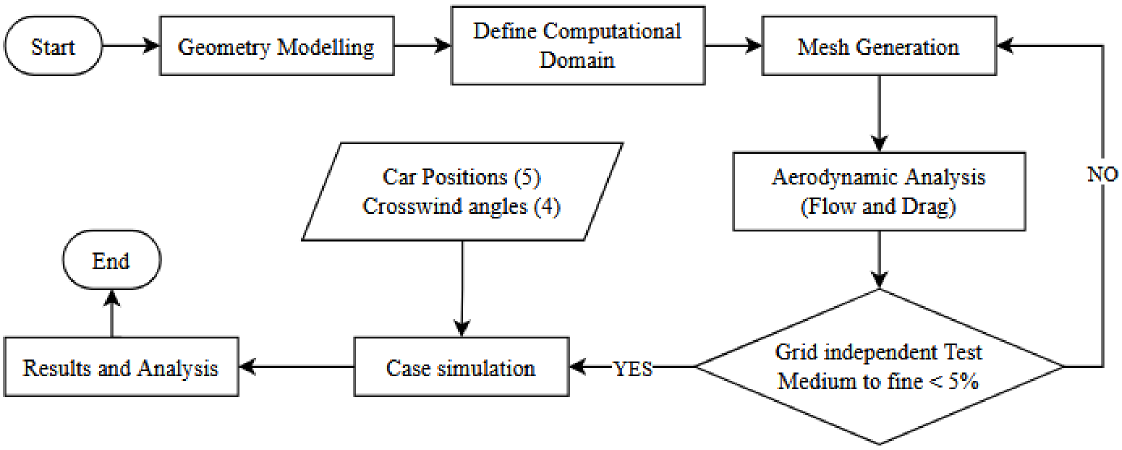

Figure 1. Flowchart of the overall CFD analysis process

The simulation investigates five overtaking stages: Case 1 (before overtaking), Case 2 (initiation), Case 3 (midpoint), Case 4 (completion), and Case 5 (post-overtaking). These cases represent progressive vehicle alignments that occur during a real-world overtaking maneuver. Crosswind conditions are simulated by applying yaw angles of 0°, 15°, 30°, and 45°, representing the effective angular deviation between the vehicle's direction of motion and the incoming wind vector. A constant inlet velocity of 110 km/h is used across all yaw angles to maintain controlled, comparable conditions. These angles represent practical crosswind scenarios commonly encountered in highway environments, ranging from calm conditions to strong lateral gusts [23]. A yaw angle of 0° corresponds to a no-crosswind (headwind) scenario and serves as the baseline for aerodynamic performance comparison. The 15° yaw angle simulates mild crosswind conditions, typically experienced during lane changes or in open road environments. A yaw angle of 30° represents a moderate crosswind situation, where aerodynamic stability may begin to deteriorate due to increased lateral loading. The 45° yaw angle reflects strong crosswind scenarios that can significantly disrupt the vehicle's stability and induce large side forces and lift fluctuations. By analyzing these specific angles, the study captures the aerodynamic trends and instabilities across a spectrum of wind intensities, which is essential for informing safety-driven vehicle design.

Although in real-world scenarios, the wind speed and direction would combine vectorially with the vehicle's velocity to form a true resultant wind angle, applying yaw angles in CFD enables simplification and direct comparison of aerodynamic coefficients at different sidewind intensities.

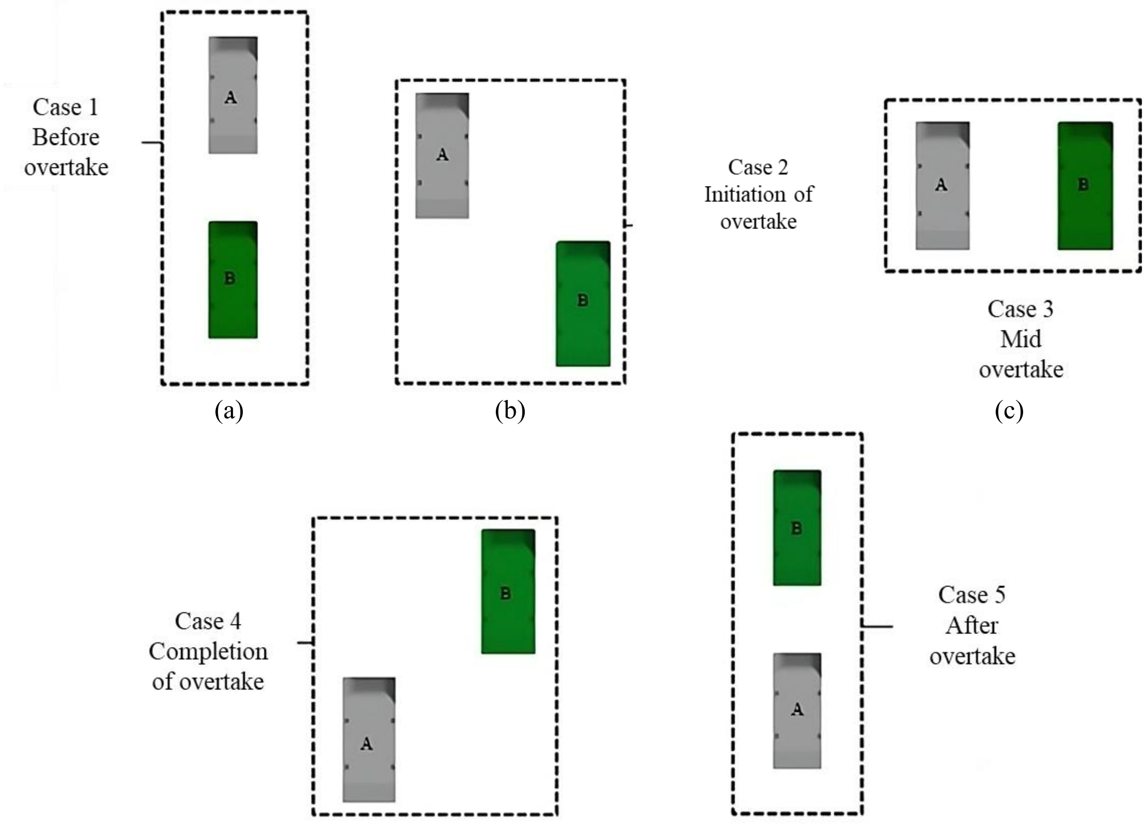

Figure 2. Different types of cases used in CFD simulation: a) Case 1, b) Case 2, c) Case 3, d) Case 4, e) Case 5

2.1 Ahmed Body Model

The Ahmed Body model is selected as the test geometry due to its ability to replicate essential aerodynamic characteristics of bluff-body vehicles while maintaining geometric simplicity and computational efficiency [24]. The model includes a slanted rear surface (25°), as in Figure 3, that induces wake separation, vortex shedding, and recirculation zones similar to those observed in real passenger vehicles [25]. Its widespread use in validation studies makes it ideal for analyzing wake dynamics and force coefficients under varying flow conditions.

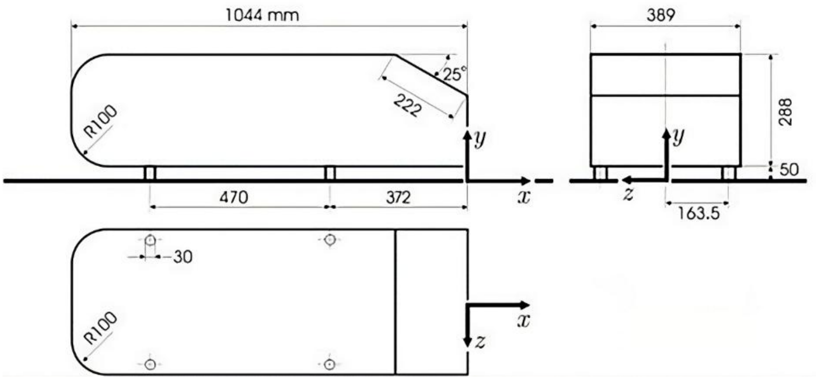

Figure 3. Ahmed Body model with dimensions (in mm)

2.2 Enclosure and Boundary Conditions

The computational domain, as shown in Figures 4 and 5, is designed to accommodate the full overtaking process between two identical Ahmed Bodies; Vehicle A (stationary or overtaken) and Vehicle B (moving or overtaking). The domain size extends 6L upstream, 10L downstream, and 5L laterally (where L is the vehicle length) to avoid blockage effects and ensure full development of wake structures.

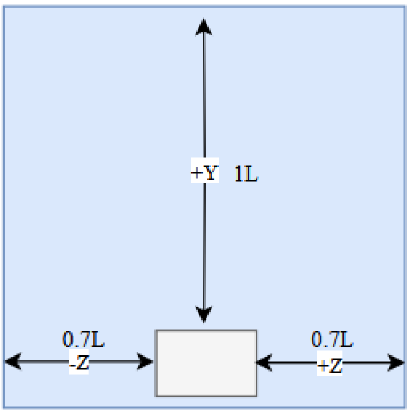

Figure 4. Enclosure for Ahmed Body in Z-axis and Y-axis

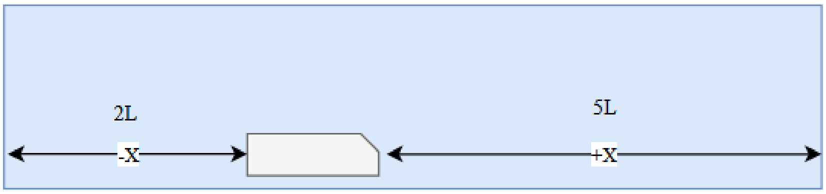

Figure 5. Enclosure of Ahmed Body in X-axis

The next stage is to name the boundaries during mesh generation. This is important in identifying surfaces in the simulation and concentrating on areas of interest, which enables a thorough evaluation of the model's reaction under various situations [26]. Defining flow conditions in a CFD simulation requires determining input and exit boundaries. In this study, the boundaries consist of a velocity inlet for the fluid's entering point, a pressure outlet for the fluid's exit, and identifying the vehicle surface for drag computation. Properly labeled boundaries are required to accurately represent fluid interactions and flow behavior. To accurately capture details such as flow gradients near the vehicle surface, boundary layer effects, and vortex formation in the wake region, the meshing element size was set to 0.025m. The mesh used in this study was an unstructured tetrahedral mesh with 10 prism layers near the wall to resolve the boundary layer. Figure 6 shows the labeled boundaries, and Figure 7 shows the mesh generated for the model.

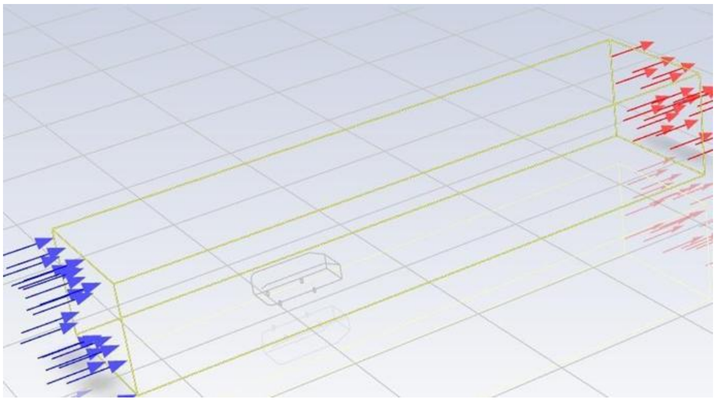
Figure 6. Inlet (blue arrow) and outlet (red arrow) before mesh generation

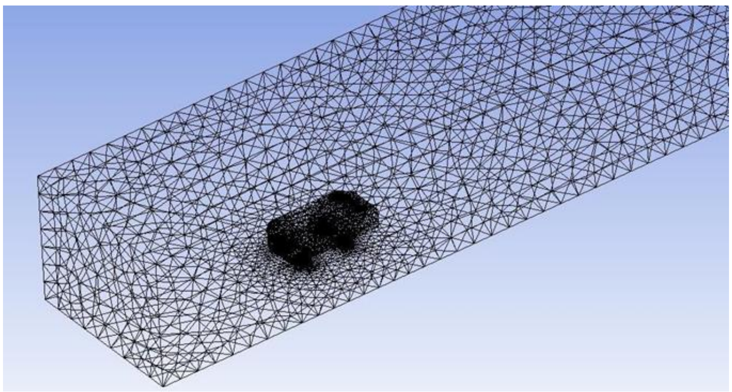
Figure 7. Mesh operation generated using ANSYS simulation

The setup operation was used to compute the model's drag coefficient. The vehicle's speed at the "velocity inlet" is determined by Malaysia's National Speed Limit Order of 1989, which ranges from 80 to 110 km/h. The grid independence test (GIT) uses a speed of 110 km/h, which is within the maximum speed range on the road. This value represents typical highway operating conditions where overtaking maneuvers frequently occur. Selecting a fixed, realistic velocity ensures that the aerodynamic responses observed in this study are directly applicable to everyday driving scenarios. This approach aligns with common practices in automotive CFD studies, where representative operating speeds are used to evaluate flow behavior and vehicle stability under standard driving conditions. The simulation's iteration number has been set to 200 to ensure that the solution converges to a stable end. The vehicle surfaces were defined using a no-slip wall boundary condition to realistically represent ground-fixed vehicle interaction with air. Additionally, the ground plane was modeled as a stationary wall to capture the effects of flow impingement and near-ground turbulence. Table 1 shows the details for boundary conditions and the values.

Table 1. Details for boundary condition and the values

Detail	Boundary Condition	Value
Inlet	Velocity Inlet	110km/h
Outlet	Pressure Outlet	0 Pa
Area of the model	Car	0.131482m
Temperature	Wall Boundary	288.16K
Symmetry	Wall Boundary	Stationary
Vehicle Body	Wall Boundary	No slip

2.3 Grid Independence Study

For numerical analysis in CFD, the target space is divided into a finite number of grids, with an optimal grid design essential for achieving precise results with the fewest number of grids [27], [28]. This includes analyzing various grid conditions. The Ahmed Body model was used to examine the grid independence, with various types and sizes of mesh resolutions tested for node count and drag coefficients (C_d). The parameters given in Table 2 compare C_d values from ANSYS simulations between the meshes. For validation, significant mesh parameters were modified, and the simulations' C_d values were compared to an earlier study by Ahmed et al. (slant angle = 25°), as shown in Table 3. Mesh 3 was chosen for the project because of its smaller cell size and lower percentage error of 3.68%, which made it more accurate than Mesh 1 and Mesh 2.

Table 1. Parameters used for grid independence test

Parameters \ Mesh type	Mesh 1 (Coarse)	Mesh 2 (Medium)	Mesh 3 (Finest)
Element size (mm)	418.81	100	30
Number of nodes	21589	40637	227892
Number of elements	111489	208306	1196761
Velocity inlet (km/h)	100	100	100
Number of iterations	200	200	200

Table 2. Comparison of drag coefficient (C_d) in different meshes with previous research

Mesh type	Drag Coefficient (C_d)	Percentage Error (%)
Mesh 1	0.334	11.71
Mesh 2	0.315	5.35
Mesh 3	0.310	3.68
Exp. by Ahmed *et al.* [29]	0.299	

Figure 8 depicts velocity contours around the Ahmed Body for three different mesh resolutions. The finest mesh (Mesh 3) reveals detailed flow features, especially in the wake region, where complex flow interactions dominate. On the slanted rear surface (25°), flow separation occurs due to an adverse pressure gradient, causing boundary layer detachment and the formation of a recirculation zone characterized by low-velocity (blue) regions. This wake is more accurately captured with finer mesh resolution, which provides sharper gradients and better resolution of vortex structures. The top and side surfaces also show the development of shear layers, particularly downstream of the body, indicating the growth of turbulent eddies in the near-wake. Mesh 1 (coarse) underpredicts these effects due to insufficient resolution, leading to a smoother, less accurate flow field. Mesh 2 improves the wake prediction, but Mesh 3 clearly resolves smaller vortical structures and more defined boundary layer separation zones. The energy loss in the wake (due to low kinetic energy and increased turbulence) is directly linked to pressure drag, which is more accurately estimated with finer meshing. The wake zone, where the air loses kinetic energy and velocity is low, is responsible for the majority of the drag force applied to the body through suction, which increases the total drag force [30].

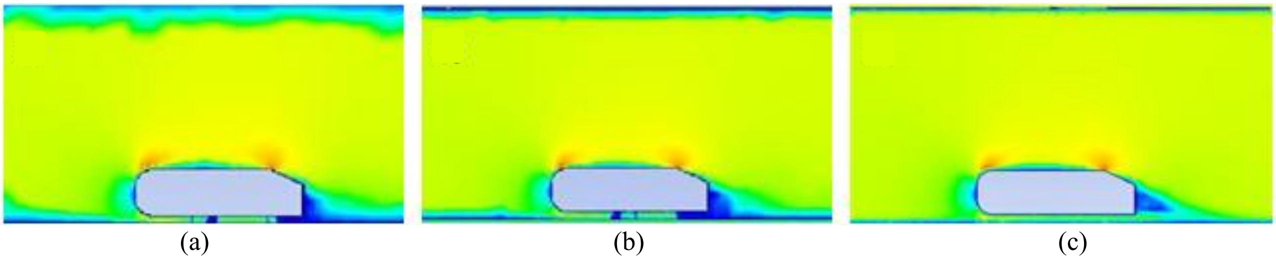

Figure 8. Comparison of velocity contour for different mesh resolutions: (a) Coarse (Mesh 1), (b) Medium (Mesh 2), and (c) Finest (Mesh 3)

2.4 Turbulence Model and Numerical Methods

The Realizable k-ε turbulence model is employed to simulate the turbulent airflow around the vehicles. This model was selected due to its enhanced capability to predict flow separation, swirling flows, and reattachment phenomena, which are highly relevant to wake dynamics during crosswind overtaking [31]. Unlike the Standard k-ε model, the Realizable version introduces an improved formulation of the turbulent viscosity and a more accurate dissipation rate equation, offering superior performance in external aerodynamic flows [32]. The governing Reynolds-Averaged Navier-Stokes (RANS) equations are discretized using a second-order upwind scheme to improve numerical accuracy. Pressure-velocity coupling is handled through the SIMPLE algorithm. Relaxation factors are carefully adjusted to ensure stable and efficient convergence [33]. The simulations are conducted under steady-state assumptions. Although transient effects exist during real overtaking, the steady-state approach is widely accepted in aerodynamic studies to analyze quasi-steady stages of the overtaking process, significantly reducing computational costs while providing meaningful force coefficient trends [34].

3. RESULTS AND DISCUSSION

The simulation setup based on real cases will be discussed briefly in this subtopic. The results were divided into two primary classifications for analysis, which are the aerodynamic loads consisting of the drag force coefficient, lift force coefficient, and side force coefficient, while the flow phenomenon consisted of flow structure, pressure distribution, and vortex formations caused by changes in velocity acting on both vehicles.

3.1 Simulations Setup Based on Real Case

Figure 9 shows the distance between two vehicles for each case based on Dong *et al*. and the Federal Highway Administration (FHWA) and National Highway Traffic Safety Administration (NHTSA) [35]. For real case simulation setup, the mesh was generated for each scenario using the Mesh 3 setup. Although the mesh used in each case has the same element size (30mm), the number of elements and nodes varies due to the cars' various positions in an overtaking scenario. The number of nodes and elements can be varied, allowing for precise resolution and improving the mesh in areas with significant flow parameters such as pressure, velocity, and flow structure. The velocity input (blue) and pressure outlet (red) are shown in Figure 10. The velocity intake allows the fluid to flow into the enclosure at various angles (0°, 15°, 30°, and 45°). The maximum number of iterations for each simulation was set to 500 based on convergence behavior observed during preliminary testing. Convergence was monitored through residuals of continuity, velocity, and turbulence quantities, all of which dropped below 1×10^{-5}. Additionally, aerodynamic coefficients (Cd, Cl, Cs) showed negligible variation (below 0.5%) after 450 iterations. As the study involved steady-state simulations using RANS equations, 500 iterations were found sufficient to achieve stable and accurate solutions. This approach balances computational efficiency and accuracy without compromising the validity of the results.

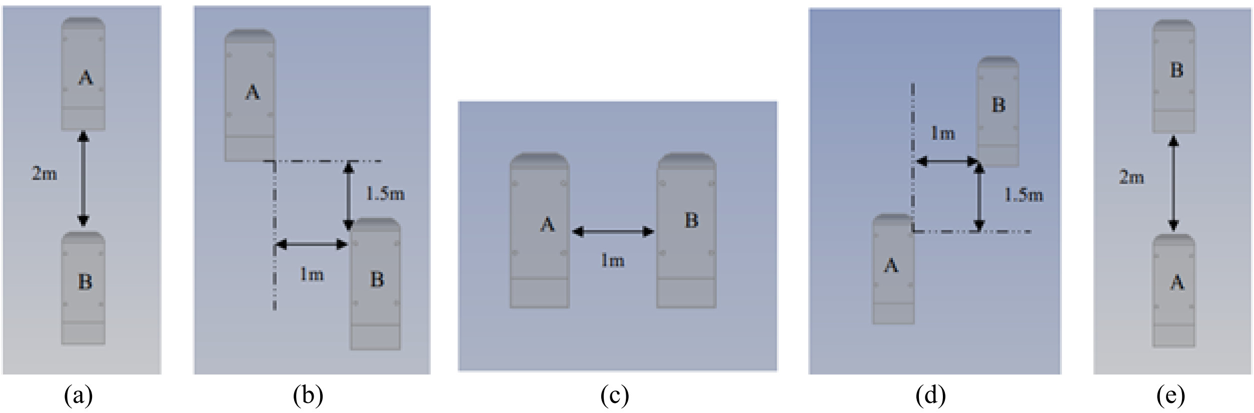

Figure 9. Distance measured between 2 vehicles(a) Case 1, (b) Case 2, (c) Case 3, (d) Case 4, and (e) Case 5

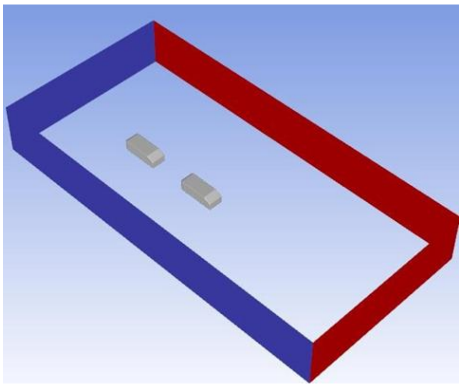

Figure 10. Velocity inlet (blue) and pressure outlet (red)

3.2 Drag Force Coefficient

Drag force is the resistive force that opposes the movement of an item through a fluid, such as air or water. It is a sort of fluid friction caused by the contact of an object and the fluid around it [36]. Figure 11 illustrates how drag coefficients (C_d) for both Car A and Car B vary under different crosswind angles and overtaking scenarios. For Car A (Figure 11(a)), the drag coefficient increases under a 15° crosswind due to greater frontal area exposure, reaching values as high as 0.3916. The drag coefficient experiences an increase primarily due to flow separation phenomena that occur as the airflow becomes increasingly skewed relative to the vehicle's longitudinal axis. This phenomenon is exacerbated by the turbulence and pressure differentials created when the wind hits the vehicle diagonally, leading to an effective increase in drag forces [37]. On the other hand, as the yaw angle approaches 30°, a different aerodynamic behavior can be observed. The drag coefficient may stabilize or even decrease after reaching this angle, indicating a transition to a different flow regime around the car [38]. Moreover, at 45°, C_d values drop significantly, especially in Case 3 (0.0159), indicating reduced pressure drag as the crosswind aligns more tangentially with the vehicle surface. For Car B (Figure 11(b)), the highest drag occurs in Case 1 at 0°, attributed to disturbed flow and frontal turbulence. Conversely, lower drag in Case 2 suggests flow streamlining due to wake interaction with Car A. At 30° and 45°, drag continues to decrease across all cases, with Case 4 reaching as low as 0.0572, implying improved aerodynamic behavior at higher yaw angles due to side-flow alignment and reduced frontal pressure.

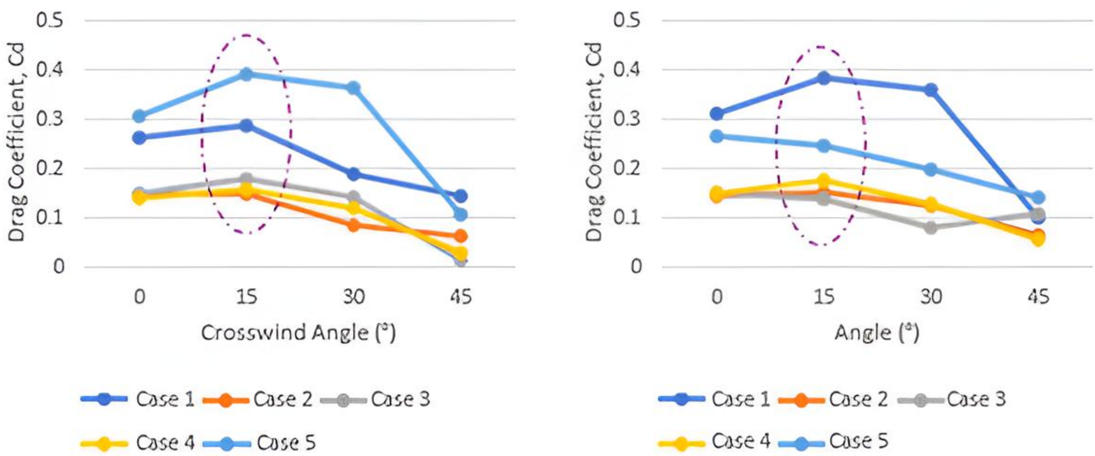

(a) (b)

Figure 11. Graph trend for different cases on drag force coefficient (C_d) in different crosswind conditions (a) Car A, (b) Car B

It can be concluded that a 15° crosswind indicates a higher drag coefficient for both of the vehicles for every case. This is due to the angle of attack of the wind relative to the vehicle surfaces, where the model's surface area is more exposed to the crosswind. Hence, a higher drag coefficient is achieved. At 30° and 45°, the wind flow might create less perpendicular pressure towards the vehicle surfaces and more parallel flow, reducing the drag force.

3.3 Lift Force Coefficient

Lift force arises due to pressure differentials created by the motion of fluid over a body, often influenced by flow curvature, separation, and vortex formation. In bluff body aerodynamics, such as with the Ahmed Body, lift can vary drastically depending on crosswind angle and the vehicle's interaction with surrounding wake structures. Importantly, negative lift may occur when low-pressure zones form on the leeward side due to vortex-induced suction, effectively pulling the vehicle downward. This phenomenon is typical when strong vortices or asymmetric flow separation dominate one side of the vehicle [39]. Figure 12 illustrates the variation of lift coefficients (C_l) for both vehicles across different overtaking cases and yaw angles. For Car A (Figure 12(a)), C_l remains relatively low at 0°, with Case 1 reaching a moderate 0.3289 due to slight flow separation at the rear. In Cases 2–4, C_l values reduce (~0.163), reflecting more stabilized flows. As the yaw angle increases to 15°, C_l values rise, particularly in Case 5, due to intensified crosswind exposure and vortex generation near the side surfaces. The highest lift for Car A is observed at 30° in Case 5, where strong turbulence and crosswind interaction with Car B's wake induce higher upwash forces and suction zones along the upper body.

At 45°, a general decline in Cl is observed, which may indicate a reattachment of flow or more streamlined side interactions that reduce lift-inducing vortices. The lift tends to decline at 45°, where flow tends to stabilize along the side, reducing vertical flow disturbances. These trends confirm that lift in crosswind-overtaking conditions is dominated by pressure asymmetry and leeward-side vortex formation. The interactions between the crosswind and the rear details of the vehicle can generate significant negative lift (downforce). Such downforce increases the load on the tires, enhancing traction and vehicle stability, but concurrently increases the drag force acting on the vehicle [40]. For Car B (Figure 12(b)), C_l is similarly low at 0°, suggesting stable longitudinal flow. In Case 5, C_l increases sharply due to downstream wake effects from Car A, which disturb the flow and create pressure imbalance. At 15°, Case 1 shows a steep increase in C_l (0.8479), possibly due to combined wake deflection and lateral vortex influence. This continues at 30°, where Case 1 peaks at 0.9436, signifying unsteady lift generation. However, Case 2 consistently exhibits lower C_l, implying more stable flow detachment and reduced lift fluctuations.

The generation of lift in these scenarios is primarily due to pressure-induced (form) drag, where flow separation and vortex strength play dominant roles. Vortex-induced lift and its unsteady characteristics directly correlate with lateral asymmetry introduced by crosswinds and overtaking maneuvers. It can be concluded that a 30° crosswind indicates a higher lift force coefficient for both of the vehicles for every case in various crosswind conditions. This is because of the crosswind angle that leads to significant flow separation and strong vortex formation on the leeward side of the vehicle. This will create low-pressure zones and increase the lift force. Research by Yudianto et al. [5] supports the notion that the side force coefficient of a vehicle increases with the lateral velocity component due to crosswind. At 15°, the vortices are less pronounced, while at 45°, the flow might reattach or form more stabilized vortices, which reduces the overall lift compared to 30°, which is a more chaotic flow.

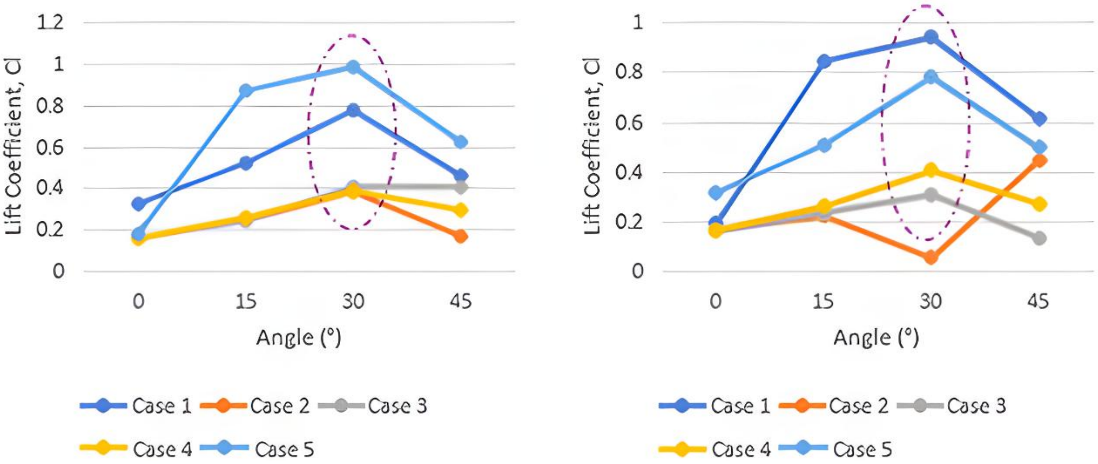

(a) (b)

Figure 12. Graph trend for different cases on lift force coefficient (C_l) in different crosswind conditions
(a) Car A, (b) Car B

3.4 Side Force Coefficient

Side force is an aerodynamic force that acts perpendicular to an object's direction of motion through a fluid, such as air or water [41]. Figure 13 presents Cs values for both vehicles across yaw angles and overtaking stages. As expected, the side force is negligible at 0° since the flow is aligned with the longitudinal axis. However, C_s increases sharply with the yaw angle. For Car B, the maximum side force occurs at 45° in Case 3, reaching a peak of 3.1192. This results from the highest cross-sectional area exposed to wind and strong leeward vortex generation, which causes significant suction on the downwind side. At intermediate yaw angles (15° and 30°), side forces vary depending on the overtaking stage. In Case 2 (initiation), Car A acts as a shield, partially blocking the wind and reducing C_s on Car B. As the vehicles align or pass, the shielding effect diminishes, and Cs increases rapidly. This dynamic nature of side force reflects the continuous evolution of pressure zones around both vehicles and is most extreme when the wake of Car A interacts directly with Car B under lateral wind loading. These findings are consistent with previous CFD and experimental studies, where side force magnitudes under strong yaw conditions were shown to dominate vehicle instability responses [42], [43].

It can be concluded that a 45° crosswind indicates a higher side force coefficient for both of the vehicles for every case in different crosswind conditions. At a 45° crosswind, the windward side of the vehicle experiences higher pressure while the leeward side experiences a lower pressure. This pressure difference is maximized at higher crosswind angles and creates strong lateral forces on the vehicles. At 15° and 30°, the pressure difference between the windward and leeward sides is less pronounced, which results in lower side force.

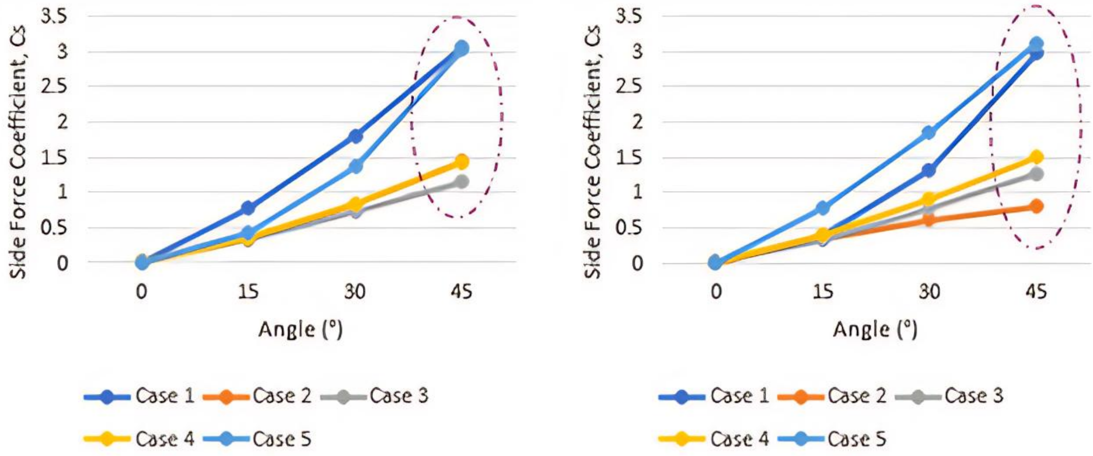

(a) (b)

Figure 13. Graph trend for different cases on side force coefficient (C_s) in different crosswind conditions (a) Car A, (b) Car B

3.5 Flow Structure in No Crosswind Conditions (ψ = 0°)

Figure 14 displays a CFD analysis of the flow dynamics during overtaking maneuvers without crosswinds, with a focus on the interaction of Car A (overtaken vehicle) and Car B (overtaking vehicle). The study uses a slice section at plane y = 0.169m through the axis to investigate specific flow properties, such as pressure distribution and vortex generation, which are critical for assessing aerodynamic stresses during overtaking. Initially, as shown in Figure 14(a), both vehicles have steady-state flow characteristics. Car A has high-pressure zones at the front, causing airflow separation and the formation of a low-pressure wake behind it. Similarly, Car B generates a low-pressure wake downstream from its frontal part. As Car B approaches Car A, as shown in Figures 14 (b) and (c), the interaction shows no significant changes in flow phenomena such as flow separation and vortex shedding as there were no crosswinds. An increasing turbulence in the wake regions occurred. This increasing turbulence causes considerable changes in airflow patterns, resulting in higher drag and aerodynamic forces on both vehicles. After executing the overtaking maneuver, the flow gradually returns to its steady state [44].

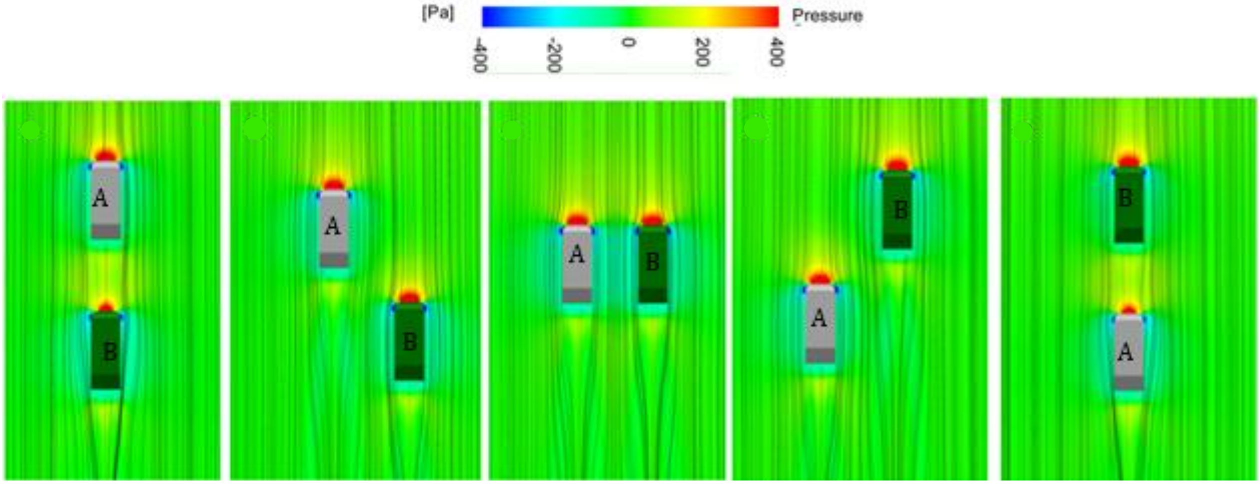

(a) (b) (c) (d) (e)

Figure 14. Flow structure for Car A and Car B for each case (a) Case 1, (b) Case 2, (c) Case 3, (d) Case 4, and (e) Case 5 at 0° angle

3.6 Flow Structure in Crosswind Conditions (ψ = 15°, 30°, and 45°angle)

In crosswind conditions, the flow structure around both vehicles becomes highly asymmetric, especially at higher yaw angles. The interaction between incoming crosswind and vehicle geometry induces shear layer separation, generating coherent vortical structures commonly referred to as eddies in the near-wake region. These vortices are primarily counter-rotating, forming due to the pressure differential between the windward and leeward sides of the vehicle. The flow structure in crosswind conditions at 15° is shown in Figure 15 and the plane cut at y-axis = 0.169m. Before the overtaking maneuver, the flow structure around Cars A and B, influenced by the crosswind, demonstrates typical features such as vortices and flow separation zones, particularly around the front corner. These interactions produce lateral displacement and yaw moments, which affect vehicle stability and aerodynamic performance. As Car B begins to overtake on the right, dynamic changes in flow structure increase lateral forces and aerodynamic disturbances. Under a 15° crosswind, Car B's lateral movement enhances vortices shed from the vehicle's edges, affecting pressure distribution and aerodynamic forces. After overtaking, the flow structure returns to a steady state, but the maneuver's effects remain. Car A's windward side faces the crosswind, resulting in increased aerodynamic loads and pressures, as seen in Figure 15 (a), while the leeward side experiences lower pressure. Car A's wake affects the leeward side of Car B, causing changes in airflow patterns and forces.

These vortices contribute significantly to aerodynamic forces, particularly lift and side force. For instance, at 30° and 45° crosswind angles, the leeward-side vortex increases suction pressure, thereby inducing negative lift and a large side force. In early overtaking stages, the presence of Car A upstream alters the wake structure of Car B, resulting in wake-wake interactions that amplify vortex strength and cause flow unsteadiness. After the overtaking is complete, these vortices migrate downstream, stabilizing over time but still contributing to lateral instability. At 30°, the pressure differential is stronger on the windward side, particularly at the front corner, whereas at 45°, high pressure occurs along the leading edge, extending from the stagnation point [45]. This high pressure is caused by the windward side immediately confronting the airflow, which converts kinetic energy to pressure energy [46]. During the early overtaking phase (Cases 2–3), Car B is in Car A's turbulent and low-pressure wake, resulting in an unstable flow condition. The flow around Car B can separate and rejoin due to the combined impacts of Car A's wake and crosswind, resulting in high pressure on the windward side as well as strong lift and side force. Vortex shedding on the windward side produces unstable aerodynamic forces. After Car B completes the overtaking maneuver (Cases 4–5), Car A's flow structure partially recovers, with the crosswind still creating lateral forces and vortices, but the wake region becomes more stable. Car B is now facing the entire force of the crosswind, resulting in significant vortices on the leeward side and flow separation on the windward side, increasing aerodynamic drag and side forces, as illustrated in Figure 16 and Figure 17. The flow structure remains complex, with vortex shedding and turbulent wake development affecting Car B’s performance.

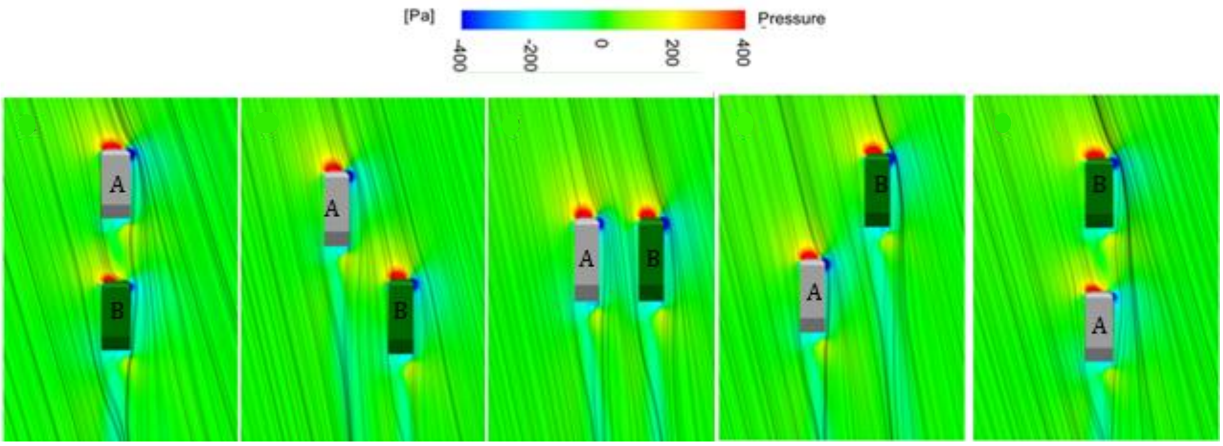

(a) (b) (c) (d) (e)

Figure 15. Flow structure for Car A and Car B for each case (a) Case 1, (b) Case 2, (c) Case 3, (d) Case 4, and (e) Case 5 at 15° angle

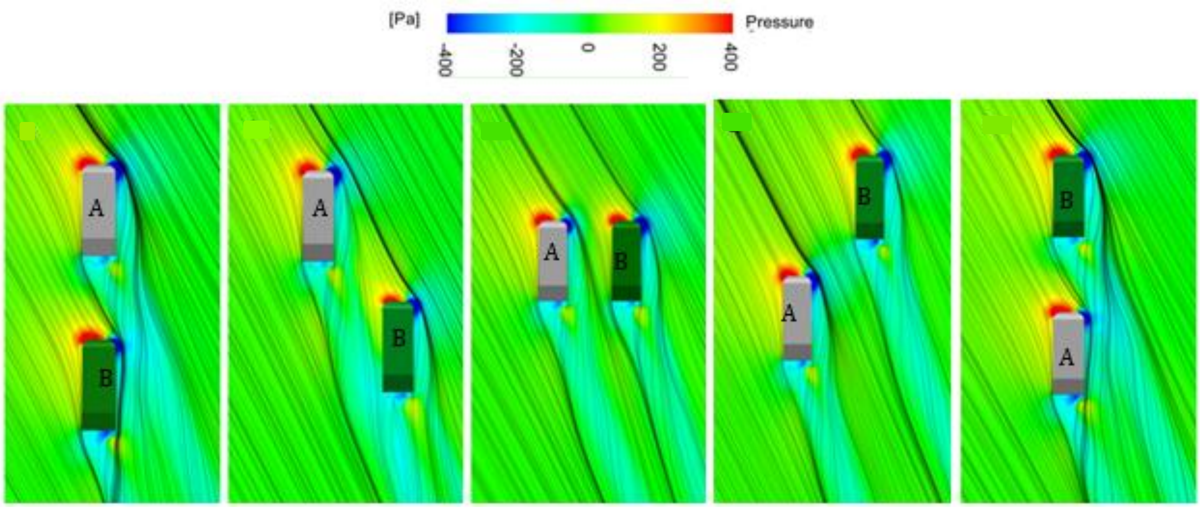

(a) (b) (c) (d) (e)

Figure 16. Flow structure for Car A and Car B for each case a) Case 1, b) Case 2, c) Case 3, d) Case 4, and e) Case 5 at 30° angle

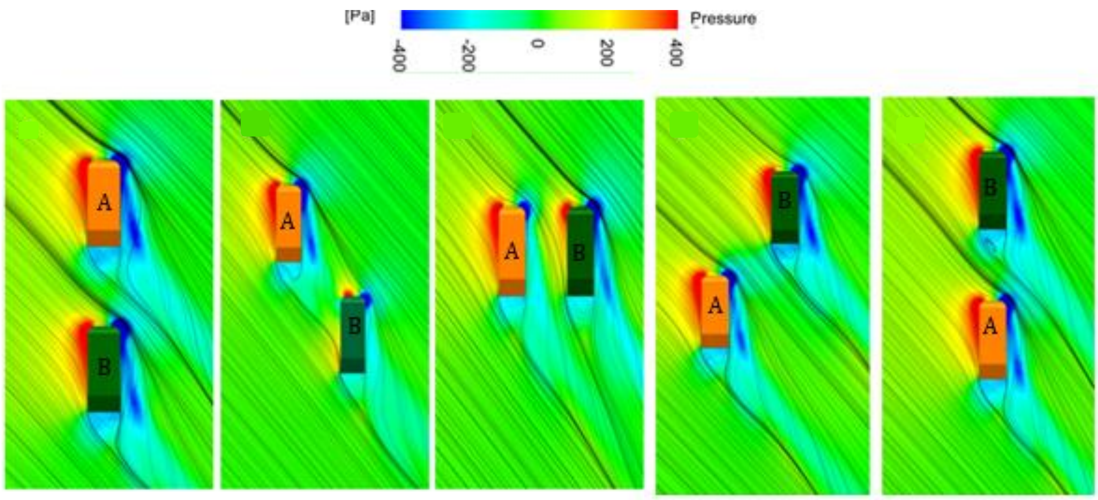

(a) (b) (c) (d) (e)

Figure 17. Flow structure for Car A and Car B for each case (a) Case 1, (b) Case 2, (c) Case 3, (d) Case 4, and (e) Case 5 at 45° angle

3.7 Pressure Contour

Due to no crosswind (0° angle), the pressure contours on both vehicles are consistent, with more pressure at the front and lower pressure at the back. However, in a 45° crosswind, Car A has higher pressure on the windward side and lower pressure on the leeward side, resulting in larger vortices. Car B in Car A's wake has lower vortex velocities due to lower crosswind pressure. During passing, as Car B approaches Car A, the pressure gradient on Car A's leeward side decreases, resulting in a turbulent wake zone that reduces side force for both vehicles. Following the maneuver, Car A returns to its original pressure difference, whereas Car B, which is now leading, has a higher pressure differential due to the crosswind. Figure 18 displays the pressure contour for cases 1, 2, and 3 at four different crosswind conditions.

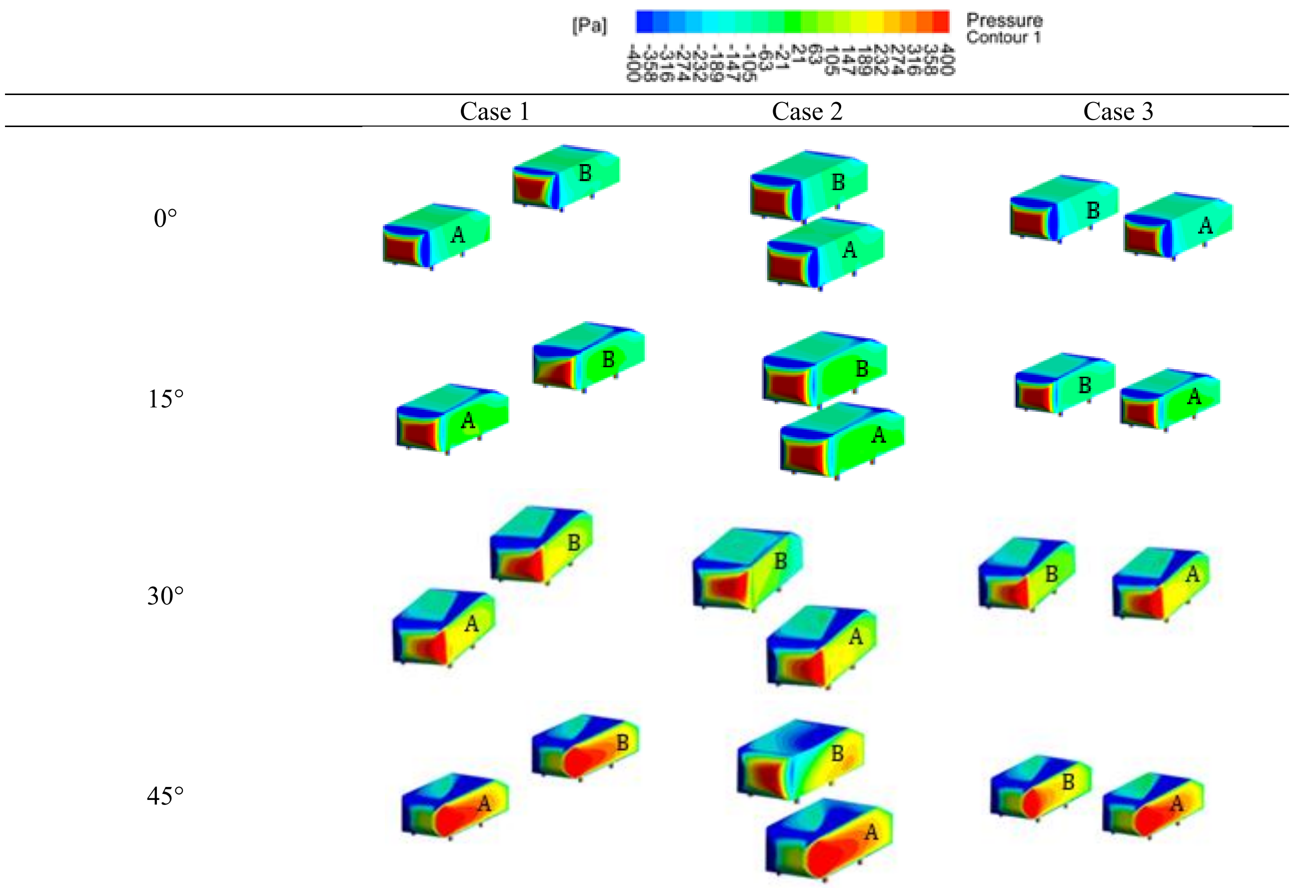

Figure 18. Pressure distribution for no crosswind conditions (0° angle) and with crosswind conditions (15°, 30°, and 45° angle)

3.8 3D Vortex Core

Figure 19 illustrates 3D vortex formation at no crosswind condition (0°) and crosswind condition (15°, 30°, and 45°) for cases 1,2 and 3. For cases 4 and 5 displays, both vehicles generate almost the same vortex as cases 1 and 2. The analysis of vortex velocity generated during overtaking maneuvers under various crosswind conditions reveals that Car B (green model) benefits from Car A's (grey model) wake at 0° crosswind, resulting in lower vortex velocities and smoother airflow due to reduced aerodynamic disturbances. As Car B begins to overtake, it confronts the disrupted vortices formed by Car A, resulting in severe aerodynamic forces. At a yaw angle of 0°, the wake remains symmetric, with two counter-rotating vortices forming behind the slanted rear of the Ahmed Body. As the yaw angle increases to 15° and 30°, the symmetry breaks down, and stronger lateral vortices emerge on the leeward side due to increased flow curvature and shear layer instability. These vortices exhibit high circulation (Γ), which can be estimated by the line integral of velocity along closed-loop streamlines. High circulation values correspond to strong rotational flow that significantly impacts local pressure fields and, consequently, lift and side force behavior.

At 45°, the vortex structures are more concentrated and deflected downstream, with large-scale separation zones forming along the vehicle's windward side. The eddies shed from the side and roof surfaces coalesce in the wake region, forming an extended low-pressure zone that amplifies side force (*Cs*) and induces suction-driven lift fluctuations. This behavior is especially prominent during the mid-overtake and side-by-side cases, where both vehicles are close enough to cause strong wake-wake interactions. In particular, Vehicle B (the overtaking car) experiences pronounced flow unsteadiness when entering the wake of Vehicle A. The resulting turbulence triggers asymmetric eddy formation that alters the boundary layer behavior, especially along the side and upper rear surfaces. These interactions lead to increased aerodynamic loading and instability, which aligns with the observed trends in side force and lift coefficients.

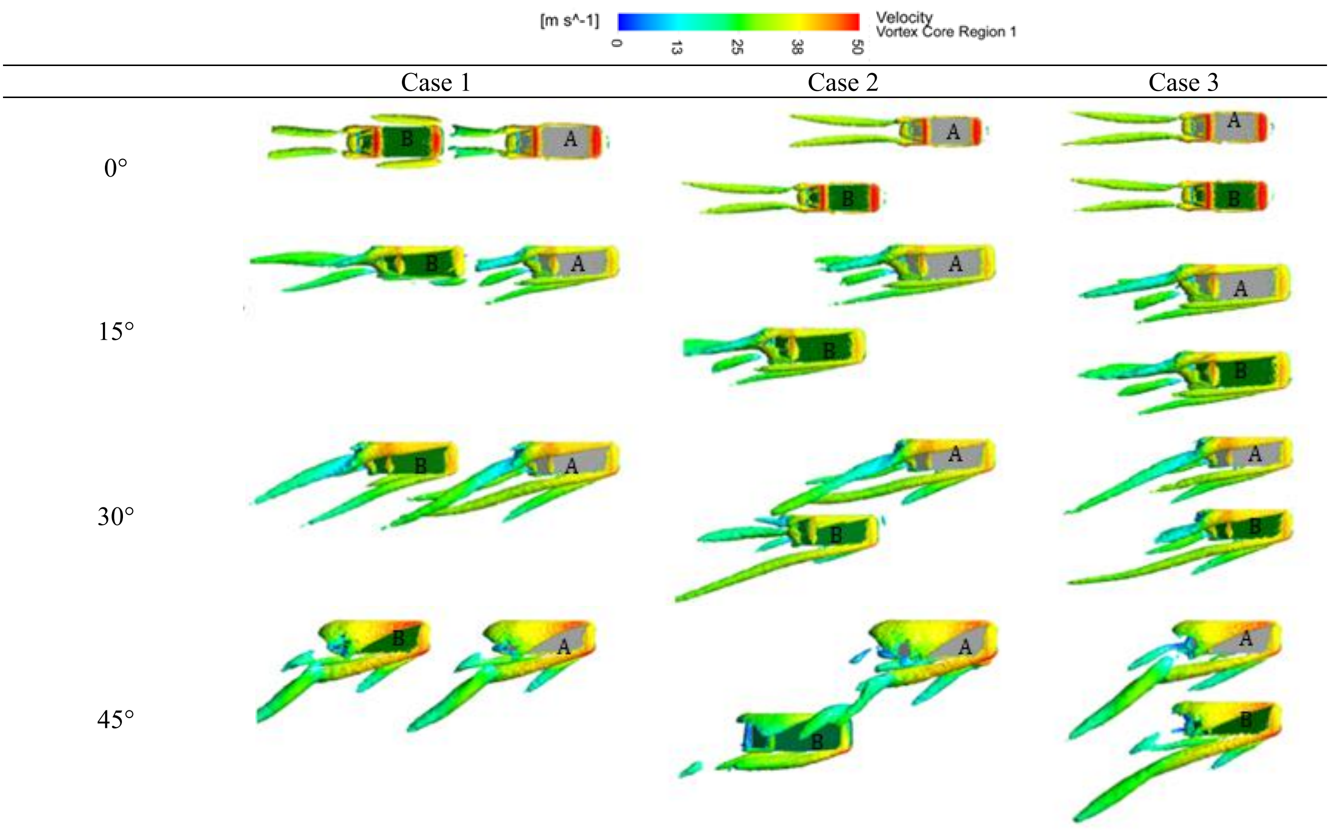

Figure 19. 3D vortex core for no crosswind conditions (0° angle) and with crosswind conditions (15°, 30°, and 45° angle)

4. CONCLUSION

This study analyzed the aerodynamic behavior of vehicles during overtaking under crosswind conditions using CFD simulations of the Ahmed Body at yaw angles of 0°, 15°, 30°, and 45°. Results showed that drag peaked at 15° due to increased frontal exposure, while lift reached its maximum at 30° because of strong leeward vortex formation. Side forces were highest at 45°, where asymmetric wake structures induced significant lateral loading, particularly during side-by-side and mid-overtake positions. Flow structure analysis confirmed the role of vortex shedding and wake deflection in generating these forces. These findings suggest that vehicle designs exposed to crosswinds should incorporate aerodynamic aids such as side skirts or rear diffusers to minimize instability. Future work may extend this study using transient simulation methods or dynamic overset mesh approaches to capture time-dependent wake interactions during actual overtaking sequences. Experimental validation under controlled wind tunnel conditions is also recommended to support the CFD findings.

ACKNOWLEDGEMENT

This research was supported by the Malaysia Ministry of Higher Education (MOHE) through the Fundamental Research Grant Scheme (FRGS/1/2020/TK02/UTHM/03/4).

CONFLICT OF INTEREST

The authors declare that they have no known competing financial interests or personal relationships that could have appeared to influence the work reported in this paper.

AUTHORS' CONTRIBUTION

M. Syafiq contributed to the conceptualization, methodology, and manuscript writing.

I. A. Ishak was involved in data analysis, supervision, and funding acquisition.

M. Arafat contributed to review editing, visualization, supervision, and funding acquisition.

R. A. Rashid contributed to data curation, while N. E. Othman assisted with resources.

Z. M. Salleh supported project administration.

S. F. Z. Abidin was responsible for review and validation.

All authors reviewed and approved the final manuscript.

REFERENCES

[1] N. Chen, H. Sun, X. Wang, and L. Zhang, "The aerodynamic characteristics of road vehicles overtaking on bridge deck under crosswinds," *Advances in Civil Engineering*, vol. 2020, no. 1, p. 8847219, 2020.

[2] W. C. Lim, I. Amin Ishak, M. Arafat, M. Nabil Farhan Kamal, N. Afzanizam Samiran, and A. Faiz Mohammad, "Analysis of the aerodynamic characteristics of small-sized car vehicles under the influence of steady crosswind," *International Journal of Application on Sciences Technology and Engineering*, vol. 1, no. 1, pp. 217–224, 2023.

[3] M. P. Ismail, I. A. Ishak, N. A. Samiran, A. F. Mohammad, Z. Mohd Salleh, and N. Darlis, "CFD analysis on the effect of vortex generator on sedan car using ANSYS software," *International Journal of Integrated Engineering*, vol. 14, no. 1, pp. 73–83, 2022.

[4] H. Sun, E. Karadimitriou, X. M. Li, and D. Mathioulakis, "Aerodynamic interference between two road vehicle models during overtaking," *Journal of Energy Engineering*, vol. 145, no. 2, p. 04019002, 2019.

[5] A. Yudianto, H. Sofyan, and N. A. Fauzi, "Aerodynamic characteristics of overtaking bus under crosswind: CFD investigation," *CFD Letters*, vol. 14, no. 8, pp. 20–32, 2022.

[6] B. J. Tayade and P. S. Bajaj, "A review on the effect of aerodynamics on car overtaking truck using CFD analysis method," *International Research Journal of Engineering and Technology*, vol. 9, no. 8, pp. 1273–1279, 2022.

[7] M. N. F. Kamal, I. A. Ishak, N. Darlis, N. M. Maruai, R. Jamian, R. A. Rashid, "Flow structure characteristics of the simplified compact car exposed to crosswind effects using CFD," *Journal of Advanced Research in Applied Sciences and Engineering Technology*, vol. 28, no. 1, pp. 56–66, 2022.

[8] M. N. F. Kamal, I. A. Ishak, N. Darlis, D. S. B. Maji, S. L. Sukiman, R. Abd Rashid, et al., "A review of aerodynamics influence on various car model geometry through CFD techniques," *Journal of Advanced Research in Fluid Mechanics and Thermal Sciences*, vol. 88, no. 1, pp. 109–125, 2021.

[9] N. Chen, X. Wang, S. Li, and H. Xiang, "Safety analysis of road vehicles overtake on cables-Stayed bridge under crosswinds," *Advances in Structural Engineering*, vol. 26, no. 5, pp. 870–887, 2023.

[10] A. Brandt, B. Jacobson, and S. Sebben, "High speed driving stability of road vehicles under crosswinds: an aerodynamic and vehicle dynamic parametric sensitivity analysis," *Vehicle System Dynamics*, vol. 60, no. 7, p. 2334-2357, 2021.

[11] C. Noger and E. Van Grevenynghe, "On the transient aerodynamic forces induced on heavy and light vehicles in overtaking processes," *International Journal of Aerodynamics*, vol. 1, no. 3/4, p. 373, 2011.

[12] D. Uystepruyst and S. Krajnović, "Numerical simulation of the transient aerodynamic phenomena induced by passing manoeuvres," *Journal of Wind Engineering and Industrial Aerodynamics*, vol. 114, pp. 62–71, 2013.

[13] C. Su, Z. Hu, Q. Zhang, X. Yuan, C. Zhang, and Y. Wang, "Coupling analysis of transient aerodynamic and dynamic response of cars in overtaking under crosswinds," *Engineering Applications of Computational Fluid Mechanics*, vol. 14, no. 1, pp. 1215–1227, 2020.

[14] T. Nakashima, C. Yan, T. Moriuchi, I. Kohri, H. Mutsuda, and Y. Doi, "Active aerodynamics control of simplified vehicle body in a crosswind condition," *The Journal of Engineering*, vol. 2020, no. 14, pp. 1005–1011, 2020.

[15] S. D. Marshall, K. Snape, D. Soper, M. Sterling, and S. Gillmeier, "The aerodynamic performance of a platoon of lorries in close-proximity during an overtaking manoeuvre," *Frontiers in Future Transportation*, vol. 5, p. 1356539, 2024.

[16] M. Tsubokura, T. Nakashima, M. Kitayama, Y. Ikawa, D. H. Doh, and T. Kobayashi, "Large eddy simulation on the unsteady aerodynamic response of a road vehicle in transient crosswinds," *International Journal of Heat and Fluid Flow*, vol. 31, no. 6, pp. 1075–1086, 2010.

[17] J. Liu, Z. Gu, T. Huang, S. Li, L. Zheng, and K. Sun, "Coupled analysis of the unsteady aerodynamics and multi-body dynamics of a small car overtaking a coach," *Proceedings of the Institution of Mechanical Engineers, Part D: Journal of Automobile Engineering*, vol. 233, no. 14, pp. 3684–3699, 2019.

[18] H. Zhou, Q. Chen, R. Qin, L. Zhang, and H. Li, "Investigation of wheelhouse shapes on the aerodynamic characteristics of a generic car model," *Advances in Mechanical Engineering*, vol. 13, no. 12, p. 16878140211066842, 2021.

[19] D. Weng, "Numerical simulations on aerodynamic drag reduction of a 25° Ahmed body by jet flow," *Science and Technology of Engineering, Chemistry and Environmental Protection*, vol. 1, no. 9, pp. 1-11, 2024.

[20] J. Sun, L. Zhang, and Y. He, "Vehicle aerodynamics characteristics of 35°Ahmed body model in crosswind conditions," *Journal of Physics: Conference Series*, vol. 2951, no. 1, p. 012036, 2025.

[21] S. S. Al Homoud, D. Harmanto, and I. Oraifige, "An investigation into the effect of drag coefficient on overtaking of car," *Applied Mechanics and Materials*, vol. 493, pp. 151–154, 2014.

[22] Z. Yuan, Z. Gu, Y. Wang, and X. Huang, "Numerical investigation for the influence of the car underbody on aerodynamic force and flow structure evolution in crosswind," *Advances in Mechanical Engineering*, vol. 10, no. 10, p. 168781401879750, 2018.

[23] M. He, S. Huo, H. Hemida, D. Soper, M. Sterling, and C. Baker, "The flow around a lorry platoon subject to a crosswind—a detached eddy simulation," *Frontiers in Future Transportation*, vol. 3, p. 901204, 2022.

[24] W. Meile, G. Brenn, A. Reppenhagen, B. Lechner, and A. Fuchs, "Experiments and numerical simulations on the aerodynamics of the Ahmed body," *CFD Letters*, vol. 3, no. 1, pp. 32–38, 2011.

[25] H. Zhou, R. Qin, G. Wang, L. Xin, Q. Wang, and Z. Zheng, "Comparative analysis of the aerodynamic behavior on Ahmed body mounted with different wheel configurations," *Proceedings of the Institution of Mechanical Engineers, Part D: Journal of Automobile Engineering*, vol. 238, no. 1, pp. 128–146, 2024.

[26] F. H. Harlow and J. E. Welch, "Numerical calculation of time-dependent viscous incompressible flow of fluid with free surface," *Physics of Fluids*, vol. 8, no. 12, pp. 2182–2189, 1965.

[27] I. A. Ishak, M. S. M. Alia, and S. A. Z. S. Salim, "Mesh size refining for a simulation of flow around a generic train model," *Wind and Structures*, vol. 24, no. 3, pp. 223–247, 2017.

[28] M. Arafat, I. A. Ishak, and A. F. Mohammad, "Influence of mesh refinement on the accuracy of numerical results for Next-Generation High Speed Train," 2023.

[29] S. R. Ahmed, G. Ramm, and G. Faltin, "Some salient features of the time-averaged ground vehicle wake," in *SAE Technical Papers*, pp. 473-503, 1984.

[30] A. Gupta, "Modeling and simulation of flow around an ahmed body using ANSYS fluent and validating result with experimental data," skill-lync.com. [Online]. Available: https://skill-lync.com/student-projects/modeling-and-simulation-of-flow-around-an-ahmed-body-using-ansys-fluent-and-validating-result-with-experimental-data

[31] C. Cravero and D. Marsano, "Computational investigation of the aerodynamics of a wheel installed on a race car with a multi-element front wing," *Fluids*, vol. 7, no. 6, p. 182, 2022.

[32] O. Mankowski, D. Sims-Williams, R. Dominy, B. Duncan, and J. Gargoloff, "The bandwidth of transient yaw effects on vehicle aerodynamics," *SAE International Journal of Passenger Cars - Mechanical Systems*, vol. 4, no. 1, pp. 131-142, 2011.

[33] Muhammad Aiman Hakim Samsuddin, "Airflow analysis of the bus under various velocities using CFD simulation," *Advanced and Sustainable Technologies*, vol. 3, no. 1, pp. 80–88, 2024.

[34] S. S. Jose and R. K. Chidambaram, "Thermal comfort optimization in an electric vehicle," *International Journal of Heat and Technology*, vol. 39, no. 6, pp. 1957–1965, 2021.

[35] D. Do Van, C.-C. Chou, and K.-C. Chang, "Numerical and experimental study of two-vehicle overtaking process," *Advances in Mechanical Engineering*, vol. 15, no. 12, p. 16878132231221044, 2023.

[36] S. Maxemow, "That's a drag: The effects of drag forces," *Undergraduate Journal of Mathematical Modeling: One + Two*, vol. 2, no. 1, pp. 1-16, 2013.

[37] K. Kurec and J. Piechna, "Influence of side spoilers on the aerodynamic properties of a sports car," *Energies*, vol. 12, no. 24, p. 4697, 2019.

[38] J. Luo *et al.*, "Research on aerodynamic characteristics of vehicle platoon under crosswind conditions based on Ahmed body," *International Journal of Numerical Methods Heat Fluid Flow*, vol. 34, no. 7, pp. 2766–2807, 2024.

[39] E. Işık, M. D. Çetin, A. Eser, and A. Yazıcı, "Analyzing of lift force to different airfoils," Technical Report, Kocaeli University, 2019.

[40] E. Guilmineau, "Effects of rear slant angles on the flow characteristics of the Ahmed body by IDDES simulations," *SAE Technical Papers*, vol. 2018, pp. 1-12, 2018.

[41] A. B. Wardlaw and A. M. Morrison, "Induced side forces at high angles of attack," *Journal of Spacecraft and Rockets*, vol. 13, no. 10, pp. 589–593, 1976.

[42] D. M. Fintelman, H. Hemida, M. Sterling, and F.-X. Li, "CFD simulations of the flow around a cyclist subjected to crosswinds," *Journal of Wind Engineering and Industrial Aerodynamics*, vol. 144, pp. 31–41, 2015.

[43] S. Rajendran, I. A. Ishak, M. Arafat, A. F. Mohammad, Z. M. Salleh, N. A. Samiran, et al., "Aerodynamic effects of high-speed train positions during tunnel exit under crosswind conditions using computational fluid dynamics," *International Journal of Automotive and Mechanical Engineering*, vol. 21, no. 2, pp. 11191–11202, 2024.

[44] J. Clarke and A. Filippone, "Unsteady computational analysis of vehicle passing," *Journal of Fluids Engineering*, vol. 129, no. 3, pp. 359–367, 2007.

[45] B. Zhang, Z. Feng, B. Xu, and T. Yang, "Efficient aerodynamic shape optimization of the hypersonic lifting body based on free form deformation technique," *IEEE Access*, vol. 7, pp. 147991–148003, 2019.

[46] F. Xu, B. Ji, Q. Xiong, G. Liu, P. Qiu, P. Xing, et al., "Numerical study on wind pressure characteristics of Chinese yurt building under downburst wind," *The Structural Design of Tall and Special Buildings*, vol. 32, no. 16, p. e2046, 2023.